Solid-State Electronics 206 (2023) 108667

Contents lists available at ScienceDirect

Solid State Electronics

journal homepage: www.elsevier.com/locate/sse

Assessment of the variability of the *I-V* characteristic of HfO_2-based resistive switching devices and its simulation using the quasi-static memdiode model

E. Salvador [a,*], M.B. Gonzalez [b], F. Campabadal [b], J. Martin-Martinez [a], R. Rodriguez [a], E. Miranda [a]

[a] Departament d'Enginyeria Electrònica, Universitat Autònoma de Barcelona, 08193 Cerdanyola del Valles, Spain
[b] Institut de Microelectrònica de Barcelona, IMB-CNM, CSIC, 08193 Cerdanyola del Valles, Spain

ARTICLE INFO

Keywords:
Memristor
Variability
Resistive switching
HfO_2

ABSTRACT

Variability of the conduction characteristics of filamentary-type resistive switching devices or resistive RAMs (RRAMs) is a hot research topic both in academia and industry because it is currently considered one of the major showstoppers for the successful development and application of this technology. In this work, we thoroughly investigate the statistics of the cycle-to-cycle (C2C) variability observed in the experimental current–voltage (*I-V*) curves of HfO_2-based memristive structures using the *fitdistrplus* package for the *R* language. This exploratory analysis allows us to identify which parametric probability distributions are the most suitable candidates for describing our data. This study involves graphical tools such as the density, skewness-kurtosis (S-K), and quantile–quantile (Q-Q) plots. The analysis is completed with the aid of goodness-of-fit statistics (Kolmogorov-Smirnov, Cramer-von Mises, Anderson-Darling) and criteria (Akaike's and Bayesian). The selected distributions are incorporated into the SPICE script of the quasi-static memdiode model for resistive switching devices and used for simulating uncorrelated C2C variability. Finally, a one-way sensitivity analysis is carried out in order to test the impact of the model parameters variation in the output characteristics of the device.

1. Introduction

Filamentary-type resistive switching devices or resistive random-access memories (RRAMs) are electroformed metal-oxide-metal structures that can alter their resistance state upon the application of an external stimulus (voltage, current, light, etc.). In these structures, a localized vacancy or ion conducting bridge spans the oxide layer and connects or disconnects the opposite electrodes in a non-volatile fashion. This means that when power is turned off, the last resistance state of the device remains unaltered. Nowadays, this kind of structure is considered a promising candidate for a plethora of applications including information storage, neuromorphic computing, logic circuits, cryptography, and many more. [1–3] Nevertheless, one of the major drawbacks that this technology must face concerns with its intrinsic variability linked to morphologic changes of the conducting filament occurring at the atomic scale [4,5]. This is particularly important for the high resistance state where a few atoms participate in the conduction process. Since variability is always present in RRAM operation, its inclusion in any compact model for such devices would be of utmost importance. In this work, uncorrelated cycle-to-cycle (C2C) variability is introduced in the quasi-static memdiode model (QMM) [6–7] through the random assignment of the model parameter values. We consider here the QMM because we are only interested in simulating the devices when subjected to ramped voltage with fixed ramp rate. For pulsed measurements, where switching times are of utmost importance, a dynamical approach is required. Uncorrelated C2C means in this context that the generated cycles are considered independent so that no trends in the low (LRS) or high (HRS) resistance state are expected. Trends can be included by adding the appropriate wearout rules in the definition of the model parameteres. The analysis reported here mainly focuses on the spread of the *I-V* curves around the median characteristic. It is worth mentioning that for specific applications, the model should be recalibrated since the parameter values may be affected by the device state history if it involves any kind of irreversible effect. After the inclusion of variability in the model parameters, the attention concentrates on the general behavior of the QMM. We have investigated how sensitive the model is

* Corresponding author.
E-mail address: emili.salvador@uab.cat (E. Salvador).

https://doi.org/10.1016/j.sse.2023.108667
Received 10 January 2022; Received in revised form 15 March 2023; Accepted 2 May 2023
Available online 11 May 2023

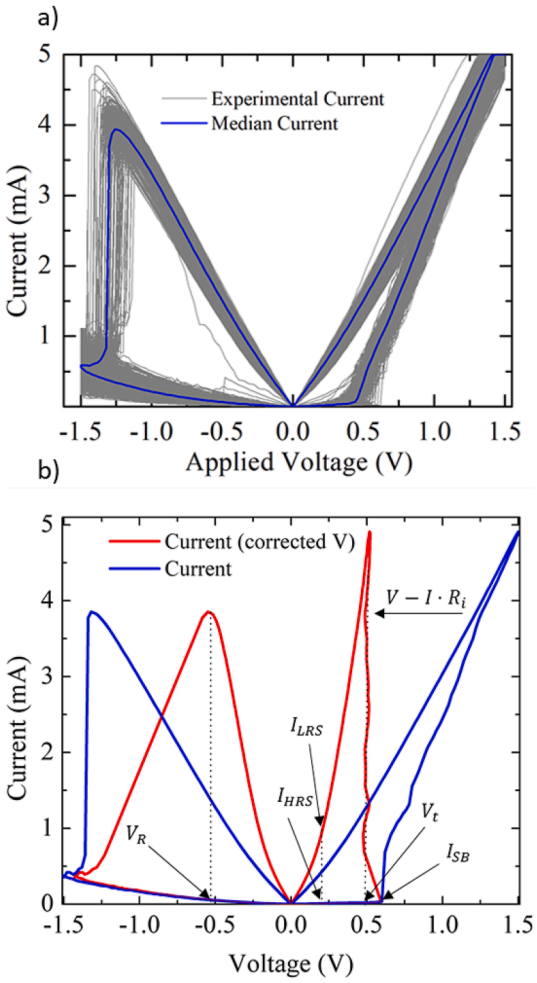

Fig. 1. A) experimental i-v curves: 450 cycles and median curve. b) voltage correction illustrating the snapback effect in a single cycle and parameter specification.

to systematic modifications of the parameter values. The approach followed is also valid for any other model and it is technically referred to as a one-way sensitivity analysis (SA). To be more precise, the sensitivity we are discussing relates to how uncertainty in the simulation output can be apportioned to different sources of uncertainty in the model inputs [8,9]. This paper is organized as follows: in Section 2, the fabrication process of the devices under investigation and the preparation of the experimental data are described. In Section 3, the experimental observations are statistically analyzed. In Section 4, the quasi-static memdiode model is presented. The inclusion of variability in the model script is discussed in Section 5. In Section 6, experimental and simulated results are compared and, in Section 7, the one-way SA is performed. Section 8 reports the conclusions of this work.

2. Devices and preparation of experimental data

The devices studied in this work are HfO_2-based metal-oxide-metal structures [10]. The oxide thickness is 10 nm and the active area of the devices is 5x5 μm^2. The bottom electrode consists in a 200 nm-thick W layer and the top electrode is a 200 nm-thick TiN layer on top of a 10 nm-thick Ti layer acting as oxygen receiver material [11]. After the electroforming process, the devices are cycled 450 times with a bipolar voltage sweep with limits $\pm$ 1.5 V. The electrical measurements were performed using the Semiconductor Parameter Analyzer (SPA) Agilent 4156C. The equipment was controlled via GPIB bus and programmed with Matlab software. The measured *I-V* curves are plotted in grey in Fig. 1.a. The median curve is plotted in blue. In Fig. 1.b, the snapback (SB) correction for a single cycle extracted from the set of experimental curves is illustrated. The snapback voltage is defined as $V_{SB} = V_{applied} - R_i \cdot I_{measured}$ where R_i is an internal series resistance (it can also include any external series resistance). The value of R_i is selected so as to provide an almost vertical increase of the current after the SET event. This vertical increase occurs at a constant voltage called the transition voltage V_T. [12] Both R_i and V_T are obtained individually for each cycle in the measurement set. A number of *observables* are indicated in Fig. 1.b: the high (I_{HRS}) and low (I_{LRS}) resistance state currents are obtained by extracting the current values at a fixed voltage, $V = 0.2$ V, the RESET voltage V_R is obtained from the voltage corresponding to the maximum current reached for negative bias. The last current data point before the SET event is the SB current I_{SB}. All these observables are extracted from the experimental curves using Matlab coding. In the following Section, the statistical distribution of these observables is investigated.

3. Analysis of the experimental results

In this Section, we investigate the statistical distribution of the observables mentioned in Section 2 using the *fitdistrplus* package for the *R* language [13]. The obtained results will be used to define the model parameters in the QMM SPICE script. First, the Cullen and Frey skewness-kurtosis (SK) or Pearson plot is used as an indicator of the appropriateness of the different candidate distributions (normal, lognormal, gamma, Weibull, logistic, etc.). This plot compares the kurtosis and the squared skewness corresponding to the available data. For some specific distributions (normal, uniform, logistic, exponential), there is only one possible value for the skewness and kurtosis. Thus, the

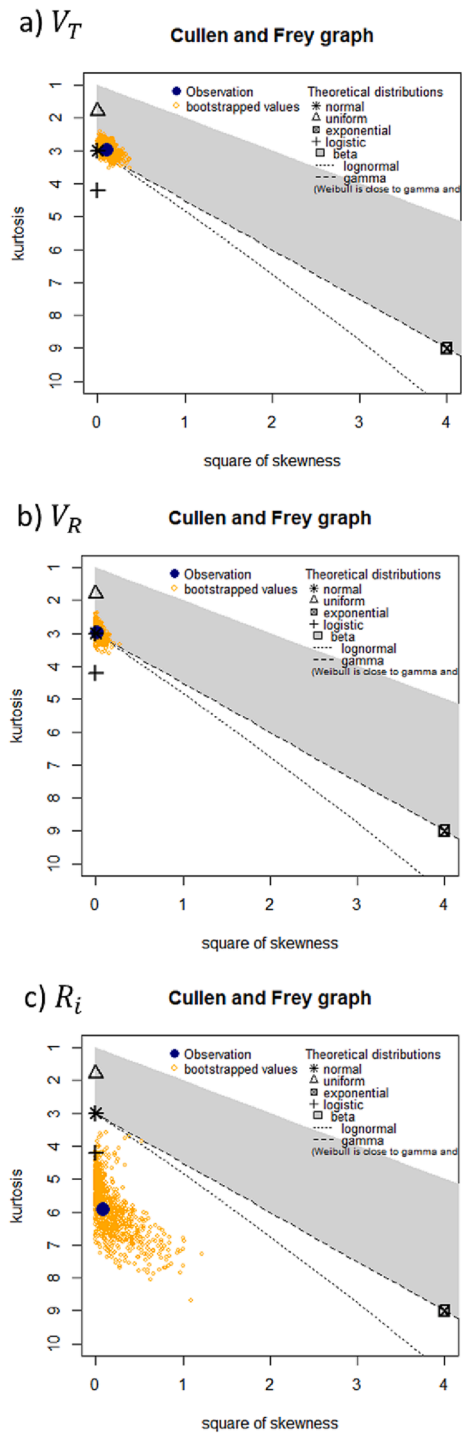

Fig. 2. A), b) and c) show the cullen and frey plots for V_T, V_R and R_i respectively.

distribution is represented by a single point on the plot. For other distributions, areas of possible values are represented, consisting in lines (as for the gamma and lognormal distributions), or shaded areas (as for the beta distribution). Notice the location of the observation (blue dot) with respect to the theoretical symbols and lines. The yellow points are bootstrapped data (random sampling with replacement). Fig. 2.a-c show the SK plot for V_T, V_R, and R_i, respectively. For V_T and V_R, the figures show that the experimental observations are close to the star symbol (normal distribution). Nevertheless, the V_T observation as well as the bootstrapping cloud are slightly shifted almost coinciding with the dashed line representing the lognormal distribution. In contrast, for R_i,

Table 1
Goodness-of-fit statistics (Kolmogorov-Smirnov, Cramer-von Mises, Anderson-Darling) and criteria (Akaike's and Bayesian) for a) V_T, b) for V_R and c) for R_I.

a)

	Method	Normal	Lognormal	Gamma	Weibull
Stat.	K-S	0.0375	**0.0295**	0.0298	0.0856
	C-vM	0.1289	**0.0576**	0.0696	0.9333
	A-D	0.9495	**0.3944**	0.5076	6.343
Cri.	AIC	-1654.55	**-1662.72**	-1661.04	-1585.18
	BIC	-1646.34	**-1654.501**	-1652.82	-1576.96

b).

	Method	Normal	Lognormal	Gamma	Weibull
Stat.	K-S	**0.0275**	0.0449	0.0393	0.046
	C-vM	**0.045**	0.1709	0.1149	0.2497
	A-D	**0.2707**	1.043	0.6944	1.858
Cri.	AIC	**-1500.53**	-1487.75	-1493.46	-1480.1
	BIC	**-1492.32**	-1479.532	-1485.25	-1471.89

c).

	Method	Normal	Lognormal	Gamma	Weibull
Stat.	K-S	**0.0954**	0.0986	0.1003	0.1532
	C-vM	**0.7561**	0.7826	0.8059	3.077
	A-D	**4.819**	4.991	5.137	18.919
Cri.	AIC	**-3315.67**	-3313.39	-3313.25	-3463.92
	BIC	**-3323.89**	-3321.62	-3321.46	-3472.14

the blue dot and the bootstrapped data show a large kurtosis (leptokurtic behavior) which means that the tails of the distribution are heavier than those corresponding to a normal distribution. Since the SK plot must only be used as a first indicator, further analysis is required before concluding which distribution better suits. Next, the different candidate distributions (normal, lognormal, gamma, and Weibull) are fitted and compared with the experimental observables. The goodness-of-fit (GoF) statistics (Kolmogorov-Smirnov, Cramer-von Mises, Anderson-Darling) and criteria (Akaike's and Bayesian) are shown in Table 1. Fig. 3.a-c show the density plots for V_T, V_R, and R_i, respectively, corresponding to the distributions investigated. The quantile–quantile (Q-Q) plots, which graphically compare the experimental distributions with the parametric models, are illustrated in Fig. 3.d-f, for V_T, V_R, and R_i, respectively. The combination of the information obtained from the GoF statistics and criteria, and the Q-Q plots were used to determine the most plausible distribution for each observable. In summary, the analysis carried out indicates that V_T follows a lognormal distribution while V_R and R_i are better described by a normal distribution. The same procedure was followed for the rest of the observables resulting in: normal distribution for I_{SB} and lognormal distributions for I_{HRS} and I_{LRS}. This information will be included in the model parameters of the QMM script and will be used to generate a set of simulated curves with variability.

4. Brief introduction to the QMM

As mentioned in Section 1, variability simulations and sensitivity analysis were performed with the QMM model [7]. This model describes the conduction characteristics of bipolar resistive switching devices

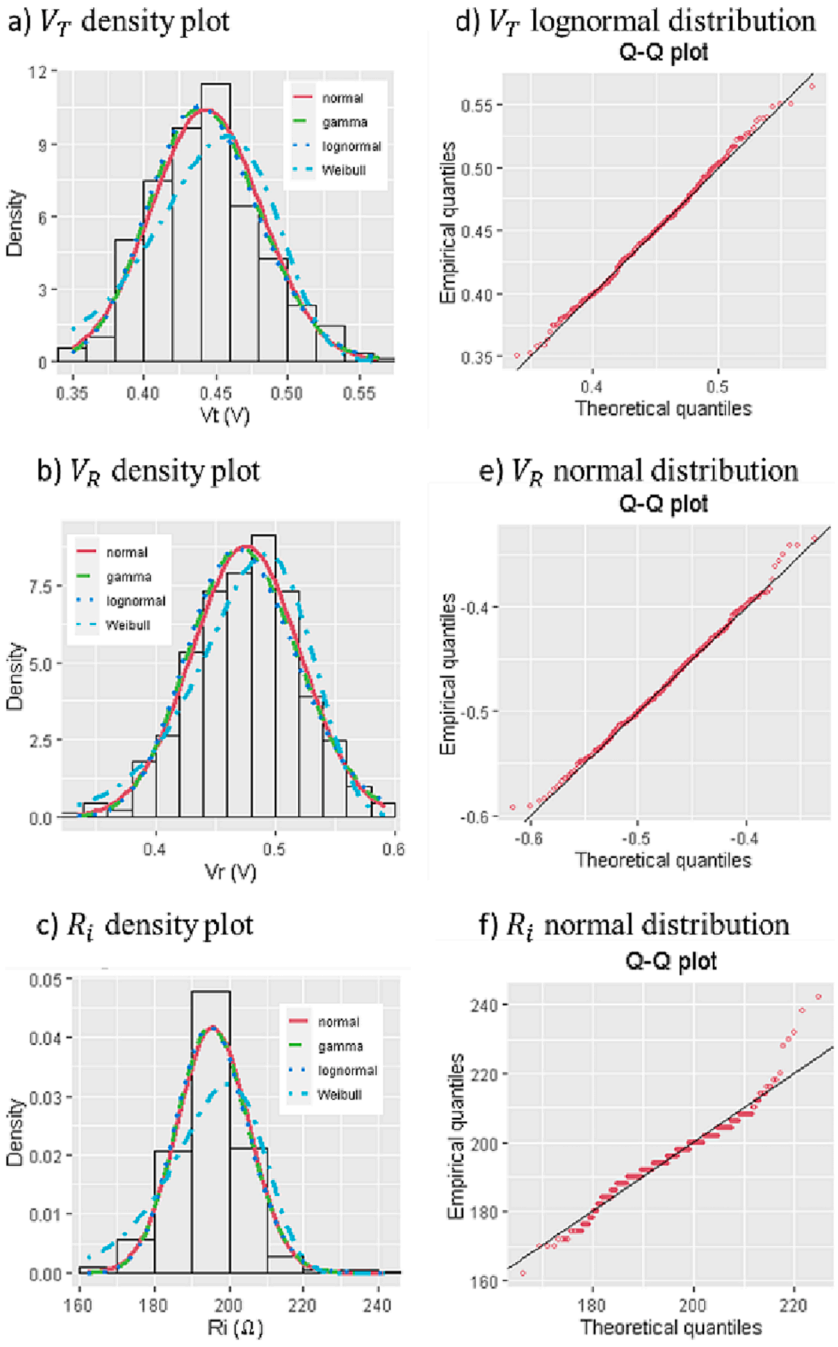

Fig. 3. A), b) and c) show density plots for V_T, V_R and R_i, respectively, with normal, gamma, lognormal, and Weibull distributions. d), e) and f) show Q-Q plots after selecting the best fitting distribution.

Table 2
LTSpice QMM script including variability in the most significant parameters taking into account the previously extracted best candidate distributions. In red the Gaussian distributions and in blue the lognormal distributions.

```
.subckt memdiode + - H
.params
+ H0=2E-3 ri=193+gauss(1) rsmin=10
+ etas=50 vs=2 etar=9 vr=-0.57+gauss(0.028)
+ rsmax=8+gauss(1) isb=33E-6+gauss(2E-6)
+ imax=exp(-5.38+gauss(0.06)) amax=2.0
+ imin=exp(-10.9+gauss(0.68)) amin=2.0
+ vt=exp(-0.733+gauss(0.08)) gam=0.07
*Memory equation
BH 0 H I=min(R(V(C,-)),max(S(V(C,-)),V(H))) Rpar=1
CH H 0 1E-3 ic={H0}
*I-V
RE + C {ri}
RS C B R=K(rsmin,rsmax)
BD B - I=K(imin,imax)*sinh(K(amin,amax)*V(B,-)) Rpar=1E10
*Auxiliary functions
.func K(min,max)=min+(max-min)*V(H)
.func S(x)=1/(1+exp(-etas*(x- if(x>isb,vt,vs))))
.func R(x)=1/(1+exp(-etar* if(gam==0,1,pow(V(H),gam))*(x-vr)))
.ends
```

using a hysteresis operator which keeps track of the memory state of the device. The origin of the switching is related to the formation of a conducting filament (CF) spanning the dielectric film caused by the application of an external field (SET process for the transition HRS to LRS). The CF is created as a consequence of the displacement and accumulation of metal ions or oxygen vacancies (depending on the device type). The CF can be ruptured by the application of a field with opposite sign (RESET process for the transition LRS to HRS). According to the QMM, the *I-V* characteristic reads:

$$I(V) = I_0(\lambda)\sinh\{\alpha(\lambda)[V - (R_S(\lambda) + R_i)I]\} \quad (1)$$

where $I_0(\lambda) = I_{0min} + (I_{0max} - I_{0min})\lambda$ is the current amplitude factor, $R_S(\lambda)$ a variable series resistance, and $\alpha(\lambda)$ a fitting parameter. I_{0min} and I_{0max} are minimum and maximum current values (same for R_S and α), respectively. According to (1), for low currents, I depends exponentially on V whereas for high currents, I depends linearly on V. Equation (2) expresses the relationship between the memory state λ and the voltage across the filament's constriction $V_C = V - R_I I$through the recursive hysteresis operator:

$$\lambda(V_C) = \min\left\{\Gamma^-(V_C), \max\left[\lambda\left(\overleftarrow{V_C}\right), \Gamma^+(V_C)\right]\right\} \quad (2)$$

where $\lambda\left(\overleftarrow{V_C}\right)$ is the memory value a timestep before (in practice dictated by the simulator timestep). Γ^+ and Γ^- are the so-called positive and negative ridge functions (sigmoidals), respectively, and are expressed as:

$$\Gamma^{\pm}(V_C) = \frac{1}{1 + \exp[-\eta^{\pm}\cdot(V_C - V^{\pm})]} \quad (3)$$

which represent the creation (+) and dissolution (-) processes of the CF. $\eta^{\pm}$ (*etas* and *etar* in the model script) are the set (+) and reset (-) transition rates and $V^{\pm}$ are the threshold voltages for set (+) and reset (-). The model uses other parameters for the fine-tuning of the simulated curves (see the script in Table 2). The model is implemented in LTspice using an equivalent circuit with behavioral current sources and includes the snapback (*isb*) and snapforward (*gam*) effects.

5. Simulation with variability using the QMM

Once the model parameter distributions were established (see Section 3), they were included in the QMM model script (see Table 2). Some of the model parameters were assumed to be constant to avoid over-randomness in the output curves. The LTspice gauss function and its transformation were used to generate the appropriate parameter values and variability. Simulations were performed having in mind the particular features of the experimental curves, such as the voltage span and the number of cycles. The parameters (including variability) are calculated at the beginning of each cycle and are kept constant until the next cycle. The goal was to reproduce as close as possible the median curve and the spread of the experimental data set. Since ultimately the simulated *I-V* curves are the result of a sequence of operations in which a number of random parameters are involved, there is always an underlying connection among the mean and dispersion values that need to be considered in order to achieve a consistent set of curves. To control this interdependence an iterative optimization process was followed to adjust the simulation parameters for obtaining close agreement with the experimental curves. The simulated observables and their variability obtained from a complete simulation run were analyzed first. With this information at hand the parameter values were modified in the appropriate direction (with the help of the one-way SA approach) and the simulation was performed again. This process was repeated until coincidence is achieved, within certain error margins, between the experimental and simulation results. Notice we included variability in 7 out of 15 model parameters, this combination was found to be reasonable for reproducing the experimental curves. For other devices, less variable parameters might be enough to reproduce their behavior, in fact a basic variable set of curves can be obtained by including the 'gauss' LTSpice function in 4 parameters (*imin, imax, isb* and *vr*).

6. Comparison between experimental and simulation results

Simulations using the QMM model were performed taking into account the iterative optimization process discussed in the previous Section. In Fig. 4, experimental (black) and simulated (blue) curves are

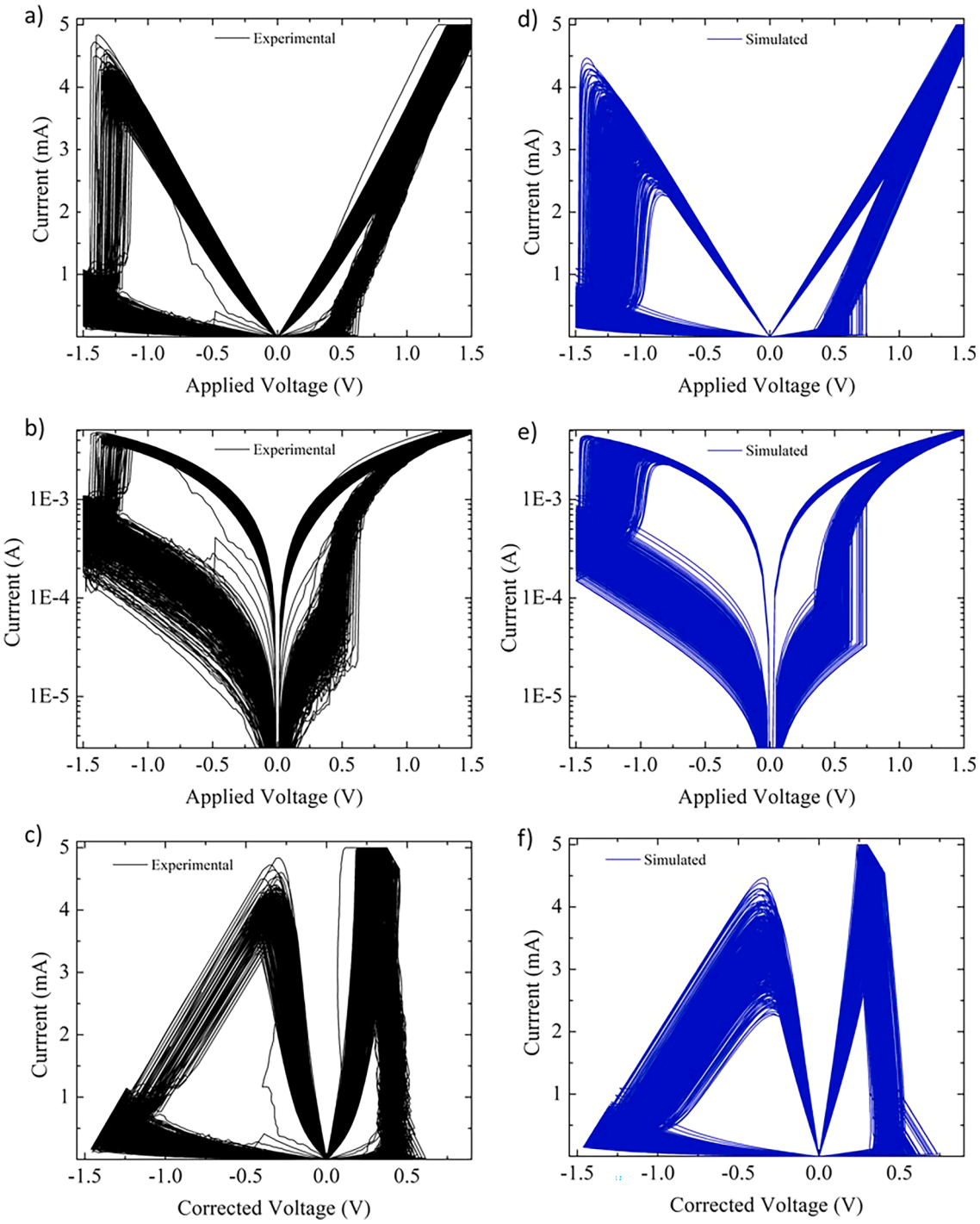

Fig. 4. Experimental and simulated curves comparison. a, d) I-V curves, b, e) I-V curves in logscale and c, f) I-V curves applying the SB voltage correction for experimental and simulated respectively.

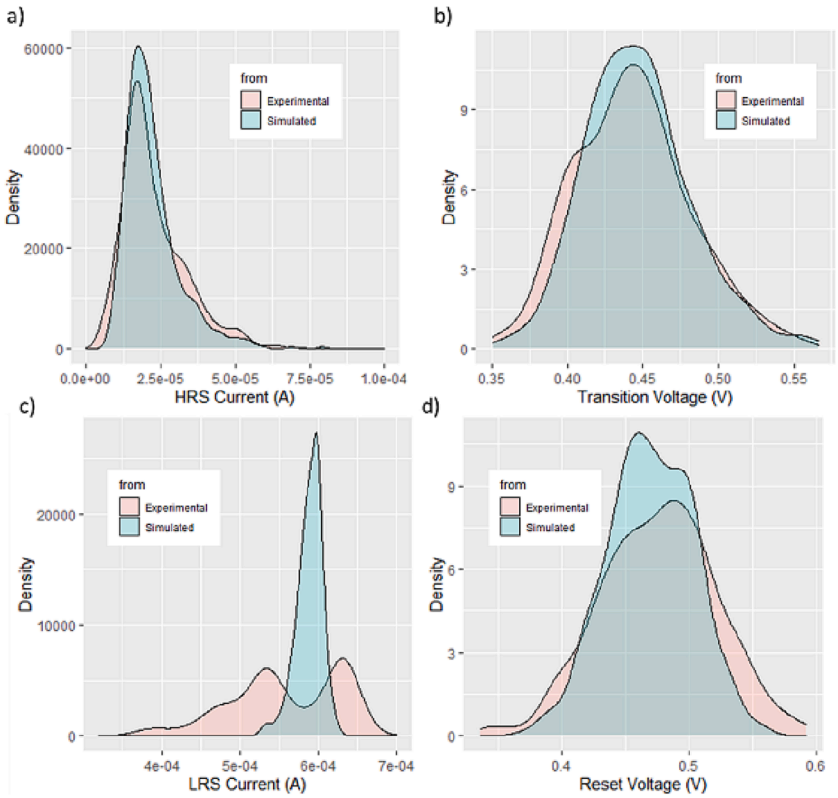

Fig. 5. Comparison of experimental and simulated parameter distributions: a) I_{HRS}, b) V_T, c) I_{LRS}, and d) V_R.

compared using three alternative plots for the same set of *I-V* curves: *a*) and *d*) linear–linear axes, *b*) and *e*) log-linear axes, and *c*) and *f*) linear–linear axes (with SB correction). The fitting is reasonably good and simulations reproduce the main features of the experimental curves in all the cases. The most conspicuous difference occurs in LRS, mainly because of a peculiarity of the available experimental data. This will be discussed later. A deeper and fairer comparison between the experimental and simulated observables is presented in Fig. 5. This figure shows the statistical distributions corresponding to the four main observables. Aiming to compile information from the different sections of the *I-V* curves, the following observables were specifically selected: I_{HRS} for the HRS curve, V_T for the SET transition, I_{LRS} for the LRS curve, and V_R for the RESET transition. This compilation was performed using the corrected *I-V* curves for V_T and V_R, and the raw *I-V* curves, i.e. without applying the SB correction for a direct evaluation of I_{HRS} and I_{LRS}. As shown in Fig. 5, the density plots corresponding to the experimental and simulated data, I_{HRS} and V_T are reproduced correctly. V_R presents a curious effect: taking a closer view at the raw *I-V* curves, the dispersion in the simulations is clearly higher than in the experimental case, but for the corrected *I-V* curves, the dispersion is well reproduced. Instead, I_{LRS} exhibits a big difference. The reason is clear, for the case under study, the experimental I_{LRS} histogram shows a double peak which likely corresponds to two different configurations of the CF or different coexisting CFs. Since the approach we are reporting here only considers a single set of parameters for each distribution, the simulated curves cannot reproduce the two distributions experimentally observed. Our parameters are only able to generate a single peak as illustrated in Fig. 5.c. This inconsistency illustrates that caution should be exercised when unexpected deviations in the experimental data occur and additional features are required to simulate them appropriately.

As an indicator of the importance of considering the time series evolution and the correlation among parameters, Fig. 6 shows experimental and simulated data corresponding to the C2C variability of two parameters: the high resistance state current *a*) I_{HRS} and the RESET voltage *b*) V_R [14]. Both figures show the presence of a trend in the experimental observables. Notice that our approach is unable to generate this trend since the LTspice simulations considered in this work do not include cross-correlation among parameters. Aiming to compare the fluctuation of the observables without trends, Fig. 6 *c*) and *d*) illustrate the difference in the observable between cycle $k + 1$ and cycle k both for I_{HRS} and V_R, defined as ΔI_{HRS} and ΔV_R, respectively. As expected, the plots show that the experimental and model fluctuations are of the same order of magnitude regardless the cycle number. In order to quantify this fluctuation, different indicators are presented in Table 3: the mean value μ, i.e. the first moment of the distribution, the standard deviation (σ), i.e. the second moment of the distribution, the interquartile range (IQR), a measures of the data spread, and the mean absolute deviation (MAD), which represents the average distance between each point and the mean value. Table 3 compares the four indicators (experimental and simulated), for the four different observables indicated in Fig. 6. It can be seen that the indicators are similar for all the observable which points out that the fluctuations are correctly captured.

7. One-way sensitivity analysis of the output curves

As mentioned in Section 1, a one-way sensitivity analysis (SA) was also carried out as part of this study. This analysis was performed considering a voltage sweep high enough to achieve the full SET and RESET states of the I-V cuves without introducing irreversible damage to the devices. To understand why the applied voltage is an important issue for this analysis, Fig. 7 illustrates the role played by the maximum applied voltage (*Vapp*) on the simulations. The figure includes indicators for the trends of the four different observables as the maximum applied voltage is increased. Notice that if the voltage is set to 1.5 V (black curve), the simulated curve does not reach the full HRS, which means that the RESET process is not complete. Therefore, if the referred voltage

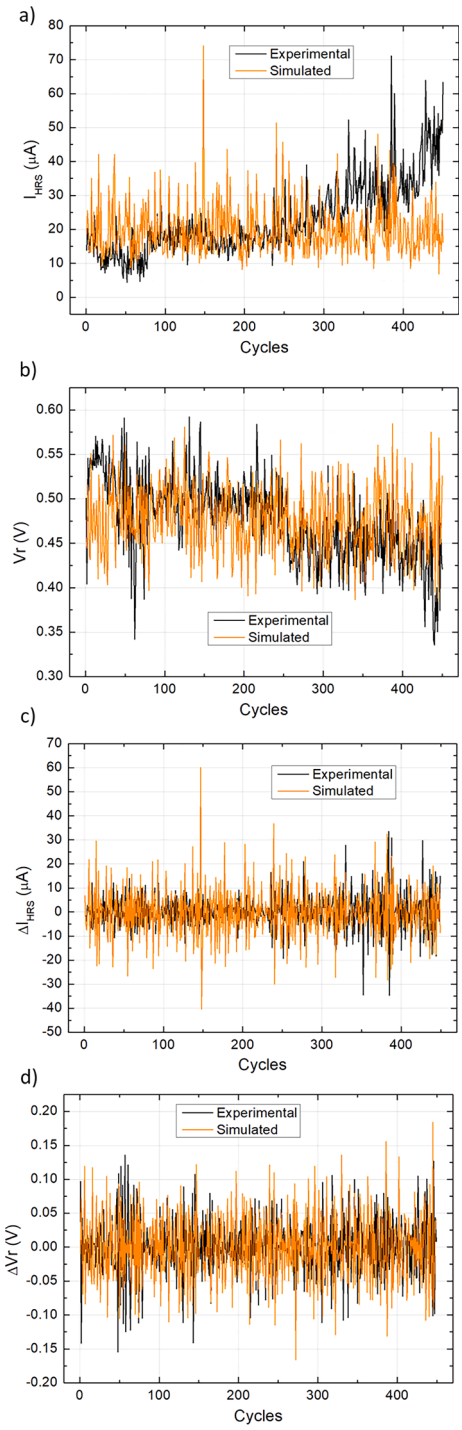

Fig. 6. Time evolution of experimental and simulated parameters for: a) HRS current, b) reset voltage, c) and d) the difference in the observable between cycle k + 1 and cycle k for I_{HRS} and V_R (ΔI_{HRS} and ΔV_R).

is not high enough, it will seriously affect the sensitivity studies performed on the rest of observables. This is an important point to consider within this analysis.

In what follows, we will only take into account complete SET and RESET processes. This can be achieved with a maximum applied voltage of ± 2.5 V (see Fig. 7 in green). The parameters were swept one at a time (50 steps each) in a reasonable range (this process does not include C2C variability) and the obtained *I-V* curves analyzed. Fig. 8 shows the relative variation of the observables as a function of the relative variation of selected model parameter: *a)* η_r or *etar* (reset transition rate), *b)* α

Table 3
Different indicators for studying the fluctuations of: HRS current, reset voltage, and the difference in the observable between cycle k + 1 and cycle k for I_{HRS} and V_R (ΔI_{HRS} and ΔV_R).

	V_R	I_{HRS}	ΔV_R	ΔI_{HRS}
Exp σ	0.0455	1.08e-05	0.0458	7.63e-06
Sim σ	0.0381	7.84e-06	0.0541	1.12e-05
Exp IQR	0.0624	1.29e-05	0.0555	7.53e-06
Sim IQR	0.0523	8.96e-06	0.0784	1.29e-05
Exp MAD	0.0455	1.08e-05	0.0458	7.63e-06
Sim MAD	0.0381	7.84e-06	0.0541	1.12e-05

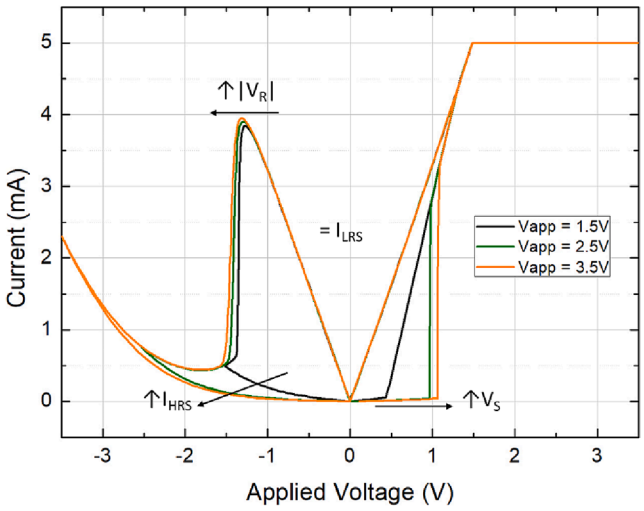

Fig. 7. Simulated I-V curves for different applied voltages. The change in the observables is indicated.

or *alpha* (*I-V* slope parameter), *c)* I_{max}, and *d)* I_{min} (maximum and minimun currents). Table 4 summarizes the magnitude and trend associated with the variation of each observable in terms of all the modified model parameters (a change of ± 30% from its reference value was considered for the analysis). The reference parameters are those obtained from the fitting of the median *I-V* curve (see Fig. 1). Notice that Table 4 uses colors and signs. Red color is associated with almost no dependence between the observable and the model parameter; orange indicates that for a 10% model parameter variation, less than 10% variation is detected in the observable and green corresponds to a variation larger than 10%. (+) or (-) indicate direct or inverse dependence, respectively. Reading the first column of Table 4, we can see the impact of all the inputs over the observable I_{HRS}. It is observed for I_{HRS} a strong and positive dependence on *alpha, Imin*, and *gam*. It also exhibits strong and inverse dependence on *Vapp* and *etar*, weak and positive effect from *Vr* and *Imax* and it is scarcely affected by *Ri*, *etas*, *Rs*, and *Isb*. This kind of test is of utmost importance for investigating the sensibility of the considered simulation model when subjected to variability.

8. Conclusions

In this work, we investigated uncorrelated C2C variability in RRAM devices using the QMM model. The analysis consisted in comparing experimental *I-V* curves, obtained from HfO_2-based devices with SPICE simulations. First, the experimental curves were analyzed and the main observables extracted. By means of the different tools available in the *fitdistrplus* package from the *R* language, the best candidate distributions for the experimental observables were determined. The obtained information was included in the model script. Simulations indicate that the QMM model can reproduce reasonably well the main features exhibited by the experimental curves in terms of mean value and variability. It was

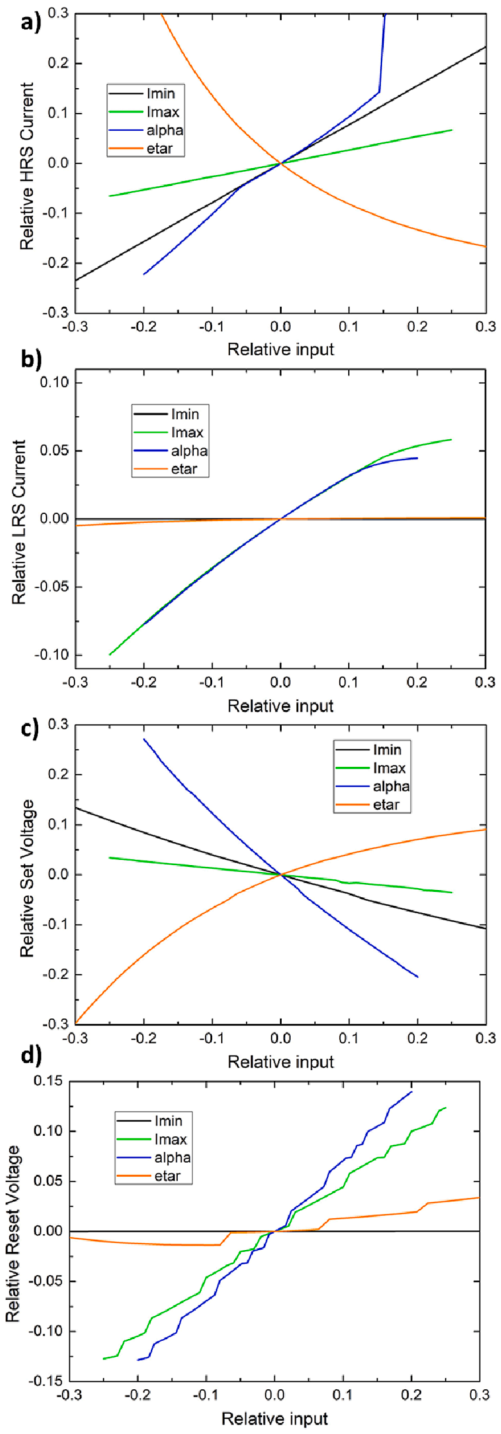

Fig. 8. One-way sensitivity plots for the relative change of the observables a) I_{HRS}, b) I_{LRS}, c) V_S and d) V_R against the relative change of the model parameters: etar, alpha, Imax and Imin.

also shown that the study of time series and chained-parameter analysis for correlated C2C variability simulations is a required action. We also investigated the impact that variations in the model inputs (parameters) have in the model outputs (observables) using a one-way sensitivity analysis. The role of each model parameter was assessed and presented graphically summarizing the intensity and detected trend between parameter and observable (direct or inverse).

Table 4
Intensity and sign (direct or opposite) of four observables against all the analyzed parameters. + and – signs for direct and inverse dependence, respectively. Green: greater than10%, orange: less than10% and red 0%.

	I_{HRS}	I_{LRS}	V_S	V_R
Vapp	-	0	+	0
Ri	0	-	0	+
etas	0	0	0	0
etar	-	0	+	+
alpha	+	+	-	+
Vr	+	0	-	+
Rs	0	-	0	-
Isb	0	0	+	0
Imax	+	+	-	+
Imin	+	0	-	0
gam	+	0	-	0

Declaration of Competing Interest

The authors declare that they have no known competing financial interests or personal relationships that could have appeared to influence the work reported in this paper.

Data availability

Data will be made available on request.

Acknowledgements

This work was supported by the Spanish Ministry of Science, Innovation and Universities through project PID2019-103869RB-C32. 'Departament de Recerca i Universitats de la Generalitat de Catalunya' is acknowledged for the 2020 FISDU 00261 grant.

References

[1] Yu S, Chen PY. IEEE Solid State Circuits Magazine 2016;8(2):43–56.
[2] J. S. Lee S. Lee, and T. W. Noh, *Appl. Phys. Rev.*, vol. 2, no. 3, 031303 (2015).
[3] Jo SH, Chang T, Ebong I, Bhadviya BB, Mazumder P, Lu W. Nano Lett 2010;10(4):1293–301.
[4] Chen A, Lin MR. IEEE IRPS 2011;843–846.
[5] A. Saltelli S. Tarantola, F. Campolongo, and M. Ratto, *John Wiley & Sons, Ltd*, (2004).
[6] Salvador E, Gonzalez MB, Campabadal F, Martin-Martinez J, Rodriguez R, Miranda E. Solid State Electron 2021;185:108040.
[7] Miranda E. IEEE TNano 2015;14:787–9.
[8] A. Saltelli , M. Ratto, T. Andres, F. Campolongo, J. Cariboni, D. Gatelli, M. Saisana and S. Tarantola, *John Wiley & Sons, Ltd*, (2008).
[9] Bargallo M, Martin-Martinez J, Maestro M, Acero MC, Nafría M, Campabadal F. IEEE Trans Electron Devices 2016;63(8):3116–22.
[10] Piccolboni G, Molas G, Garbin D, Vianello E, Cueto O, Cagli C, et al. IEEE Electron Device Lett 2016;37(6):721–3.
[11] Poblador S, Gonzalez MB, Campabadal F. Microelectron Eng 2018;187–188:148–53.
[12] Karpov V, Niraula D, Karpov I. Appl Phys Lett 2015;109:1–5.
[13] Delignette-Muller ML, Dutang C. J Stat Softw 2015;64:1–34.
[14] Alonso FJ, Maldonado D, Aguilera AM, Roldán JB. Chaos. Solitons and Fractals 2021;143:110461.

Emili Salvador Aguilera Is a PhD student at the Electronical Engineering department from the Universitat Autònoma de Barcelona under the supervision of Enrique Alberto Miranda and Rosana Rodríguez, from the same department. Prior to the PhD, coursed my Bachelor degree in Nanoscience and Nanotechnology and Master degree in Advanced Nanoscience and Nanotechnology at the Universitat Autònoma de Barcelona. He carried out my Master thesis at the Institut Català de Nanociència i Nanotechnology (ICN2) working in the graphene transistors field.

Mireia Bargallo Gonzalez received the degree in physics from the University of Barcelona, Barcelona, Spain, and the Ph.D. degree on the topic of stress analysis and defect characterization techniques of semiconductor materials and devices, from Katholieke Universiteit Leuven, Leuven, Belgium, in 2011. She pursued her Ph.D thesis with the Interuniversity Microelectronics Center (imec), Leuven, Belgium. In 2011, she joined the Institut de Microelectrònica de Barcelona (IMB-CNM, CSIC). Her current research interests include electrical characterization, modeling and applications of resistive switching devices.

Francesca Campabadal received the Ph.D. degree in physics from the Universitat Autònoma de Barcelona, Bellaterra, Spain, in 1986. She joined the Institut de Microelectrònica de Barcelona, Consejo Superior de Investigaciones Científicas, Barcelona, Spain, in 1987, where she is currently a Research Professor. Her current research interests include the deposition of high-k dielectric layers, their electrical characteristics, and the resistive switching phenomena in RRAM devices.

Javier Martin-Martinez Javier Martin-Martinez received the M.S. degree in physics from the Universidad de Zaragoza, Zaragoza, Spain, in 2004, and the Ph.D. degree from the Universitat Autònoma de Barcelona (UAB), Bellaterra, Spain, in 2009. He was with the Università degli Studi di Padova, Padua, Italy, and IMEC, Leuven, Belgium. He is currently an Associate Professor with UAB. His main research interests include the characterization and modeling of failure mechanisms in MOSFETs and also RRAM characterization and modeling for neuromorphic applications.

Rosana Rodriguez received the Ph. D. in Electrical Engineering from Universitat Autonoma de Barcelona (UAB) in 2000. Funded by the Fulbright program, she worked on devices and circuits reliability at the IBM Thomas J. Watson Research Center (USA). Currently, she is associate professor at the UAB. Her research is focused on the variability and reliability of advanced CMOS devices. She is interested in the electrical characterization and modeling of process-related and time–dependent variability sources as Random Telegraph Noise (RTN) and aging mechanisms as Bias Temperature instability (BTI) and Hot Carrier Injection (HCI). Her research includes the study of the variability impact on the performance of single devices and digital and analogical circuits. She is also interested in the characterization of resistive switching devices (memristors) and their application for non-volatile memories, computing and neuromorphic applications.

ENRIQUE MIRANDA is Professor at the Universitat Autonoma de Barcelona (UAB), Spain. He has a PhD in Electronics Engineering from the UAB (1999) and a PhD in Physics from the Universidad de Buenos Aires, Argentina (2001). He received numerous scholarships and awards including: RAMON y CAJAL (UAB), DAAD (Technical University Hamburg-Harburg), MATSUMAE (Tokyo Institute of Technology, Japan), TAN CHIN TUAN (Nanyang Technological University, Singapore), WALTON award from Science Foundation Ireland (Tyndall National Institute), Distinguished Visitor Award (Royal Academy of Engineering, UK), CESAR MILSTEIN (CNEA, Argentina), Visiting Professorships from the Abdus Salam International Centre for Theoretical Physics, Slovak Academy of Sciences, Politecnico di Torino, Leverhulme Trust (University College London, UK), and Nokia Foundation (University of Turku, Finland). He serves as member of the Distinguished Lecturer program of the Electron Devices Society (EDS-IEEE) since 2001 and as Associate Editor of Microelectronics Reliability since 2003. He has authored and co-authored around 250 peer-review journal papers.